aerospace

MDPI

Article

Effects of Ozone Addition on Multi-Wave Modes of Hydrogen–Air Rotating Detonations

Yang Wang [1], Cheng Tian [1,*] and Pengfei Yang [2]

[1] School of Aerospace Engineering, Beijing Institute of Technology, Beijing 100081, China; yangwang_bit@163.com
[2] SKLTCS, CAPT, Department of Mechanics and Engineering Science, College of Engineering, Peking University, Beijing 100871, China; young1505@foxmail.com
* Correspondence: chengtianbit@outlook.com

Abstract: Ozone addition presents a promising approach for optimizing and regulating both combustion and ignition mechanisms. In Rotating Detonation Engines (RDEs), investigating the impact of ozone addition is particularly important due to the fact of their unique operating conditions and potential for improved efficiency. This study explores the influence of ozone concentration, total temperature, and equivalent ratio on the combustion characteristics of a hydrogen–air mixture infused with ozone. Utilizing the mixture as a propellant, the combustion chamber of a continuous rotating detonation engine is replicated through an array of injection ports, with numerical simulations conducted to analyze the detonation wave combustion mode. Our results show that an increase in total temperature leads to an increase in the number of detonation waves. Incorporating a minor quantity of ozone can facilitate the ignition process for the detonation wave. Increasing the ozone content can result in the conversion from a single-wave to dual-wave or multi-wave mode, providing a more stable combustion interface. A low ozone concentration acts as an auxiliary ignition agent and can significantly shorten the induction time. As the total temperature increases, the detonation propagation velocity and the peak heat release rate both decrease concurrently, which leads to a decline in the exit total pressure and an augmentation in the specific impulse. Employing ozone exerts a minimal impact on the detonation propagation and the overall propulsion performance. The requirement for ozone-assisted initiation differs noticeably between rich and lean combustion.

Keywords: Rotating Detonation Engine (RDE); ozone; combustion mode; numerical simulation

Citation: Wang, Y.; Tian, C.; Yang, P. Effects of Ozone Addition on Multi-Wave Modes of Hydrogen–Air Rotating Detonations. *Aerospace* **2023**, *10*, 443. https://doi.org/10.3390/aerospace10050443

Received: 4 April 2023
Revised: 28 April 2023
Accepted: 5 May 2023
Published: 11 May 2023

1. Introduction

Detonation is a type of combustion characterized by the rapid propagation of a shock wave and combustion surface, which can reach speeds of kilometers per second. Detonation-based combustion, which boasts a high thermal cycle efficiency and a lower increase in entropy, has gained heightened interest in recent times. Several types of heat engines that utilize detonation combustion have been studied, including Pulse Detonation Engines (PDEs), Oblique Detonation Engines (ODEs) [1], and Rotating Detonation Engines (RDEs) [2–4]. However, the performance of a PDEs is significantly impacted by its intake system, limiting its operating frequency due to the need for repeated ignitions. The major challenge of oblique detonation engines is maintaining a stable oblique detonation, despite its wider flight range and higher thermal cycle efficiency. In contrast, the Rotating Detonation Engine (RDE) is designed with a continually fed chamber of fuel and oxidizer, ensuring the circumferential propagation of the detonation. To ensure continuous operation, RDEs operate at higher frequencies than PDEs, resulting in a more stable performance than ODEs/PDEs. This results in a more straightforward structure and higher thermal efficiency compared to traditional combustion systems [5–7].

The concept of a continuous detonation engine has been studied since the 1960s [8]. By the 1980s, Bykovskii [9–11] successfully realized rotating detonation combustion using

liquid and common gaseous fuels, such as hydrogen, methane, and propane, as propellants based on prior experimentation. Zhou and Wang [12] conducted numerical studies on the RDEs and found that the flow field variation along the radial direction is not significant when the chamber width is small. Yi [13] evaluated the impact of various design parameters, such as the injection area ratio and chamber length, on the propulsive performance. Uemura [14] studied the process of transverse wave generation from the intersection between the detonation front and the burnt gas mixture region. They used two-dimensional and three-dimensional numerical simulations to clearly demonstrate the rotating detonation propagation mechanism and dynamics in RDEs. Ma [15] conducted experimental research on RDEs focused on ignition, quenching, re-initiation, and the stabilization process in a reactant injector array. They observed the transition of rotating detonation waves. They found that the re-initiation phenomenon is related to the injection pressure of the propellant. Furthermore, some studies have explored the impact of factors, such as total pressure [16], thrust efficiency [17], nozzle design [18–20], and tail nozzle characteristics [21,22]. Owing to the ignition challenges associated with large-molecule fuels, Zhang [23] utilized the addition of hydrogen to facilitate auxiliary detonation. Kindracki et al. [24,25] used kerosene/air as reactants and studied the propagation characteristics of rotating detonation waves in gas–liquid two-phase systems by adding hydrogen as a combustion enhancer. Zhao et al. [26] numerically studied the effects of equivalence ratio, initial pressure, and temperature on the instability of n-heptane/air detonation waves. The performance of a rotating detonation combustion chamber is related to the propagation mode of the detonation waves in the chamber. Fotia et al. [27] studied the effect of the tail pipe structure on the performance of a rotating detonation combustion chamber.

Zhao [28] conducted experimental research on the low-temperature oxidation chemistry of dimethyl ether (DME), with ozone as an oxidant. Han [29] studied the effects of adding O_3 to an H_2/O_2 mixture to investigate the changes in the initiation and propagation of detonation waves by using numerical simulations. Ozone has been utilized as an accelerant in partially accelerated and controlled combustion [30]. The integration of ozone significantly alters the ignition process without altering the mixture properties. Previous studies have investigated various aspects of RDEs, including their flow field variations, design parameters, and propagation mechanisms. To prevent the high temperatures from burnt products, inert diluents are introduced into the fuel–oxidizer mixture, leading to a longer induction length and time. This can significantly affect the rotating detonation structure. Considering the ignition difficulties associated with certain fuels such as propellants, the idea of adding O_3 to the propellant aims to improve the detonation within the RDEs. However, limited research has been conducted on the use of ozone in RDEs. Therefore, it is essential to investigate the addition of ozone to RDEs propellants.

This study aimed to investigate the impact of ozone addition on rotating detonation waves using a hydrogen–air mixture. Specifically, two-dimensional numerical simulations were used to vary the total temperature, ozone content, and reactant equivalence ratios to analyze the effects on thrust performance and detonation wave propagation.

2. Materials and Methods

To investigate two-dimensional rotating detonation combustion, the multispecies Navier–Stokes equations method was adopted as the governing equations. The equations are expressed as:

$$\frac{\partial \rho}{\partial t} + \frac{\partial \rho u_j}{\partial x_j} = 0 \tag{1}$$

$$\frac{\partial \rho u_i}{\partial t} + \frac{\partial \rho u_i u_j + p\delta_{ij}}{\partial x_j} = \frac{\partial \tau_{ij}}{\partial x_j} \tag{2}$$

$$\frac{\partial \rho e}{\partial t} + \frac{\partial \rho u_j e + P u_j}{\partial x_j} = \frac{\partial \rho u_j \tau_{ij}}{\partial x_j} + \frac{\partial}{\partial x_j}\left(\frac{k\partial T}{\partial x_j}\right) + \frac{\partial}{\partial x_j}\left(\sum_k \rho D h_k \frac{\partial Y_k}{\partial x_j}\right) \tag{3}$$

$$\frac{\partial \rho Y_k}{\partial t} + \frac{\partial \rho Y_k u_j}{\partial x_j} - \frac{\partial}{\partial x_j}\left(\rho D \frac{\partial Y_k}{\partial x_j}\right) = \dot{w}_k \tag{4}$$

where t is time; δ_{ij} is the Kronecker delta; ρ, u, p, e, T, h_k, and Y_k are the density, velocity vector, pressure, specific total energy, temperature, enthalpy of the k-th component, and mass fraction, respectively, with the viscous stress tensor, τ_{ij}, calculated using:

$$\tau_{ij} = \mu\left(\left(\frac{\partial u_i}{\partial x_j} + \frac{\partial u_j}{\partial x_i}\right) - \frac{2}{3}\frac{\partial u_k}{\partial x_k}\delta_{ij}\right) \tag{5}$$

where μ is the viscosity, and w_k is the reaction rate of the k-th species. The diffusion coefficient, D, is obtained from the Schmidt number and viscosity.

The chemical kinetic model employed in this work is based on the comprehensive H_2/air mechanisms of Burke [31], which includes 19 species and 32 reactions, together with an O_3 submechanism consisting of eight steps [28]. To solve the equations, an implicit Euler time integration method was utilized, along with the KNP (Kurganov, Noelle, and Petrova) scheme [32], known for its stability and efficiency in shock capturing. The van Leer limiter was adopted for correct flux calculations.

The physical model used in this study was a simplified 2D schematic of an annular RDE chamber, represented as a rectangular computational domain (see Figure 1). The width of the chamber is much smaller than the diameter of the combustion chamber and can be unrolled circumferentially. The propellants are fed in premixed via the sonic nozzles arranged at constant intervals along the bottom boundary, with the outlet assumed as a nonreflective boundary with a backpressure of 1 atm and ambient temperature of 300 K. The left and right ends of the domain are treated as periodic boundaries.

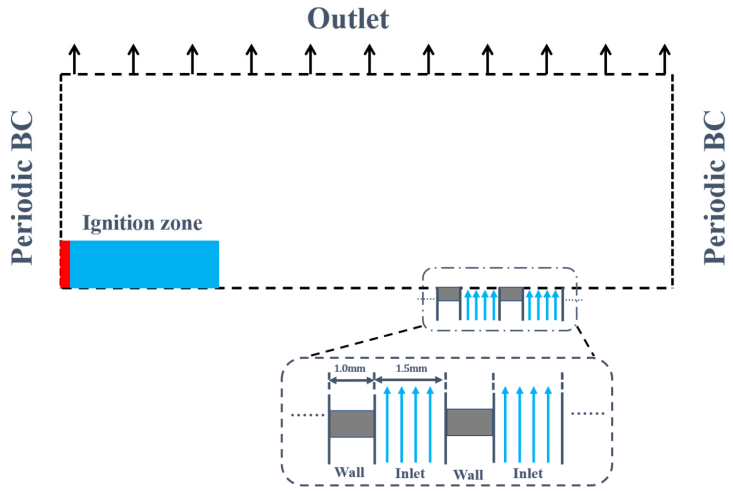

Figure 1. Schematic of the initiation of rotating detonation waves.

The computational domain contains 1000 × 300 cells in the x- and y-directions. The circumferential length (x-direction) and axial length (y-direction) of the domain were 100 mm and 50 mm. The ratio between the maximum and minimum grid sizes in the y-direction was 3, while the length of the cell in the x direction was fixed at 100 µm. At the initial time, a high-temperature and high-pressure red area was placed at the bottom of the domain, with blue premixed gases in front of the spot. The rest of the space was filled with air at ambient pressure and temperature.

The injector conditions were computed assuming isentropic expansion through a sonic nozzle into the combustion

- For $p \geq p_{st}$, there is no inflow, the sonic nozzle is chocked, where p_{st} is the inlet total pressure;

- For $p_{st} > p > p_{cr}$, the speed of inflow can be obtained by isentropic expansion:

$$T = T_{st}\left(\frac{p}{p_{st}}\right)^{\frac{\gamma-1}{\gamma}}$$

$$u = \sqrt{RT_{st}\frac{2\gamma}{\gamma-1}\left[1-\left(\frac{p}{p_{st}}\right)^{\frac{\gamma-1}{\gamma}}\right]} \quad (6)$$

  where T and T_{st} are the temperature and the total temperature of the inlet flow; γ is the specific heat ratio; and R is the gas constant of the reactants;
- For $p \leq p_{cr}$, the sonic nozzle is chocked, $p = p_{cr}$, and the temperature and velocity are computed using Equation (4).

The critical pressure, p_{cr}, is defined according to the stagnation pressure and specific heat ratio:

$$p_{cr} = p_{st}\left(\frac{2}{\gamma+1}\right)^{\frac{\gamma}{\gamma-1}} \quad (7)$$

In order to explore the effect of ozone addition on rotating detonation waves, we defined φ as a measure of ozone content:

$$\varphi = \frac{X_{O_3}}{X_{H_2} + X_{O_2} + X_{N_2} + X_{O_3}} \quad (8)$$

Here, X_i denotes the volume fraction of the gases. The variable φ is varied in the simulations to investigate the impact of ozone on RDEs. Different mesh resolutions were evaluated using various grids, with the maximum size ranging from 0.05 mm to 0.10 mm. In this paper, we determined that the detonation wave had reached a stable state when the average wave speed approached a steady value, as measured by adding pressure monitoring points. This method is consistent with the usual experimental approach for determining the formation of stable detonation waves. Figure 2a shows the temperature contour for different grids when the flow field reached a steady state with a total temperature of 300 K, total pressure of 0.5 MPa, and φ = 1.0%. Figure 2b compares the distribution of temperature and pressure variations along the *x*-direction at different heights for two different mesh resolutions. Both grids generally predict similar flow structures and circumferential pressure variations. To ensure the accuracy and reduce the computational time, a mesh resolution with a maximum size of 0.1 mm was used for the simulations.

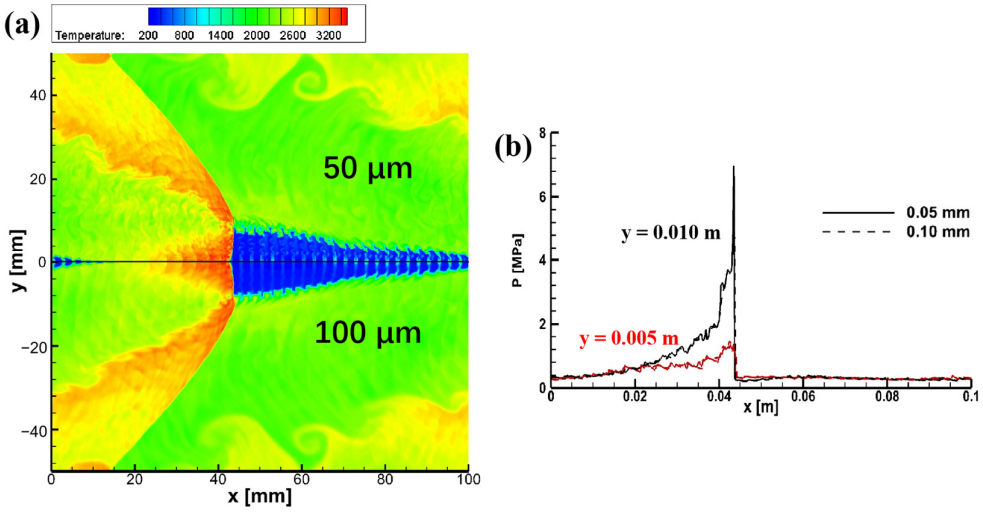

Figure 2. (**a**) Temperature fields; (**b**) along the line y = 0.005 m and y = 0.010 m; based on different grids for T_{st} = 300 K and φ = 0.1%.

3. Results

3.1. Effects of Total Temperature on the Modes of Detonation

To investigate the impact of ozone on rotating detonation waves under various total temperature conditions, some basic cases were conducted with the inlet total temperature ranging from 300 K to 600 K. The width of the inlet and wall areas were set to 1.5 mm and 1.0 mm, respectively, with a chemical equivalent ratio of H_2/air. The sonic nozzle was evenly distributed at the bottom, with an inlet total pressure of 0.5 MPa.

Total temperature can be divided into static temperature and dynamic temperature. Due to the presence of walls in the case, as the total temperature increased, the temperature and velocity of the inflow at the inlet nozzle also increased. Figure 3 shows the evolution of the temperature field with varying total temperatures. At a total temperature of 300 K, a single detonation wave was present in the flow field, but it was weakened near the wall due to the recirculation zone of the combustion products (Figure 3a). The combustion surface and the shock surface began to decouple, as shown in Figure 3b. It was obvious that the combustion surface near the inlet area disappeared completely, as shown in Figure 3c. At a total temperature of 400 K, only one detonation wave was present in the flow field, as shown in Figure 3d. Although the detonation wave underwent multiple cycle repetitions, the fresh premixed gas ahead of the wave in the flow field formed irregular triangular structures. Similar results were obtained in previous experimental findings for this self-adjusting detonation wave [33]. As the total temperature increased to 500 K, dual waves were observed to propagate in the same direction, as shown in Figure 3e,f. In general, the number of detonation waves increased as the total temperature rose, which is consistent with Yao [34].

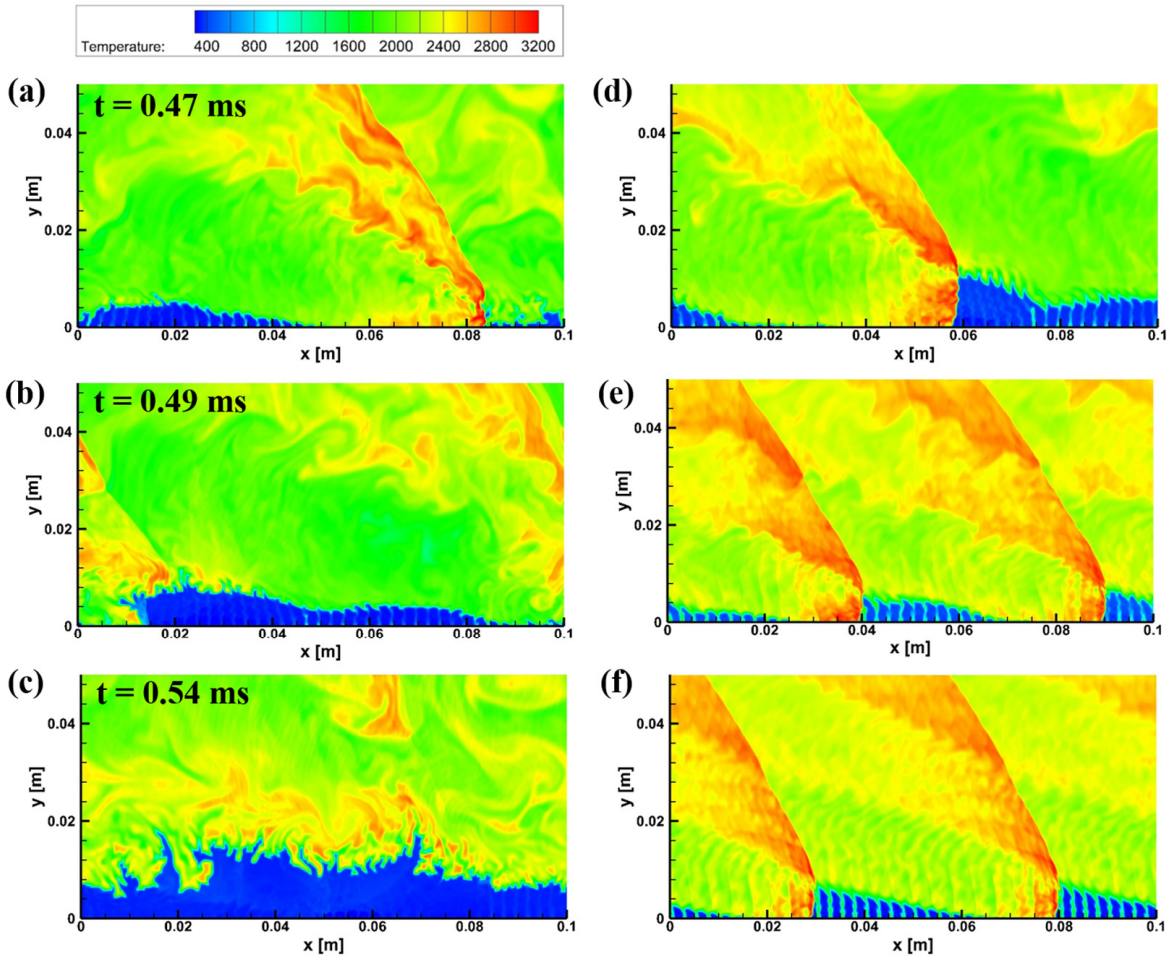

Figure 3. Temperature fields of RDW with (**a**–**c**) T_{st} = 300 K; (**d**) 400 K; (**e**) 500 K; (**f**) 600 K.

3.2. Effects of Ozone Addition

To investigate the impact of ozone addition on rotating detonation waves, simulations were conducted with different ozone content values ranging from 0.1% to 2.0% at a total temperature of 300 K. Ozone was added to the premixed inflow, and there was no mixing process. Due to the presence of walls, the actual distribution of ozone was the same as the distribution of hydrogen, which formed a banded pattern ahead of the detonation wave.

Figure 4 shows the temperature distribution at different ozone content values. At an ozone content of 0.1%, a rotating detonation wave (RDW) was successfully initiated, with a sawtooth structure observed on the contact surface (Figure 4a). This structure is thought to be related to the absence of fresh gas injection near the wall. When the ozone content increased to 1.0%, the RDW remained a single wave, with the sawtooth structure still visible on the contact surface (Figure 4b). The sawtooth structure was more prominent near the surface (S1) closer to the detonation wave, while surface (S2) was smoother. At an ozone content of 2.0%, the simulation showed a dual-wave mode, with no visible sawtooth structure on the contact surface (Figure 4c). Overall, these results suggest that increasing the ozone content can improve the initiation of rotating detonation waves, with a sawtooth structure being observable on the contact surface at lower ozone content values. The observed discontinuities in the contact surface are caused by the nonuniform characteristics of the incoming flow. Ozone plays a role in assisting ignition and even changing the propagation mode of detonation waves.

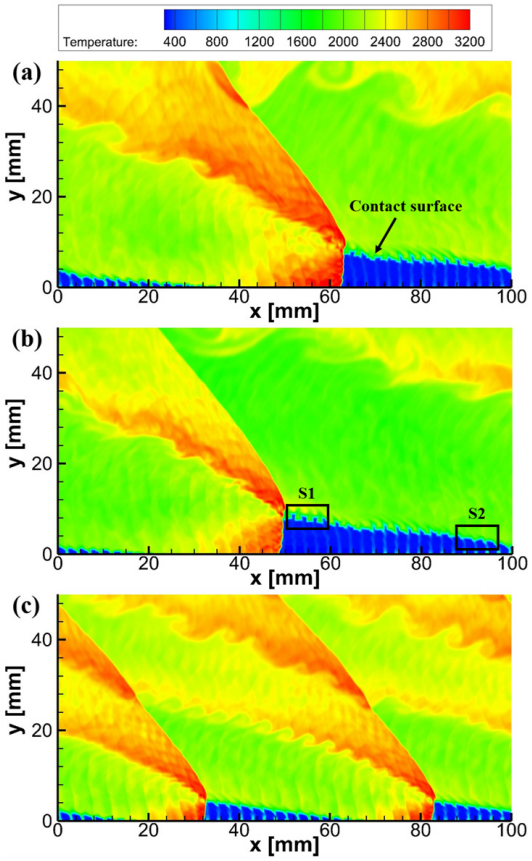

Figure 4. Temperature fields at T_{st} = 300 K with different ozone additions: (**a**) φ = 0.1%; (**b**) φ = 1.0%; (**c**) φ = 2.0%.

Additionally, we found that at a total temperature of 400 K, after monitoring the propagation of the detonation wave for a long time, the speed of the detonation wave no longer exhibited significant changes. The same type of self-adjusting single-wave results could be obtained, as shown in Figure 5a. The height of the gas in front of the detonation wave changes noticeably, with L2 greater than L1. This change in height is related to the

amount of fresh gas ahead of the wave. When there was less fresh gas, the detonation wave became weaker. At the location of L1, the detonation wave became weaker than the balance state. The accumulation of unburnt gas led to a stronger detonation wave, which reduced the amount of fresh gas that could be injected into the chamber. At φ = 1.0%, a transition in the number of detonation waves was observed, as shown in Figure 5b. In the case of the dual-wave mode at a total temperature of 400 K, increasing the ozone content resulted in a smoother contact surface. This suggests that the ozone content can have a significant impact on the structure and behavior of rotating detonation waves, and the flow field displays a more stable multi-wave structure under conditions of relatively high total temperature.

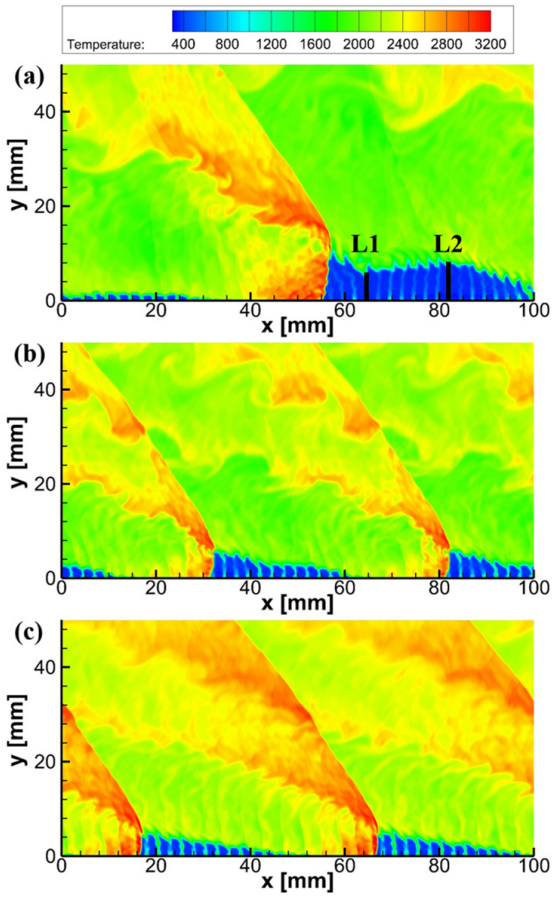

Figure 5. Temperature fields at T_{st} = 400 K with different ozone additions: (**a**) φ = 0.1%; (**b**) φ = 1.0%; (**c**) φ = 2.0%.

Figure 6a illustrates the temperature distributions at φ = 0.1%. It is evident that the burnt products obtained from the previous round of propagation were trapped within the intervals of the injection nozzles. These burnt products, which have higher temperatures, were distributed uniformly in the fresh gas region in a banded form. In Figure 6b,c, the stable triple-wave mode was calculated at φ = 1.0% and φ = 2.0%. This suggests that to induce a transition in the propagation mode under the condition of a higher total temperature inflow, a higher ozone concentration is required. As shown in Figures 5 and 6, there were banded regions of combustion products ahead of the detonation wave, which is consistent with the experimental observations by Gamba et al. [35], and this is commonly referred to as parasitic combustion. It was observed that the parasitic combustion region became larger as the total temperature increased. In fact, parasitic combustion is an energy loss mechanism [36,37] that can reduce the overall efficiency of the engine.

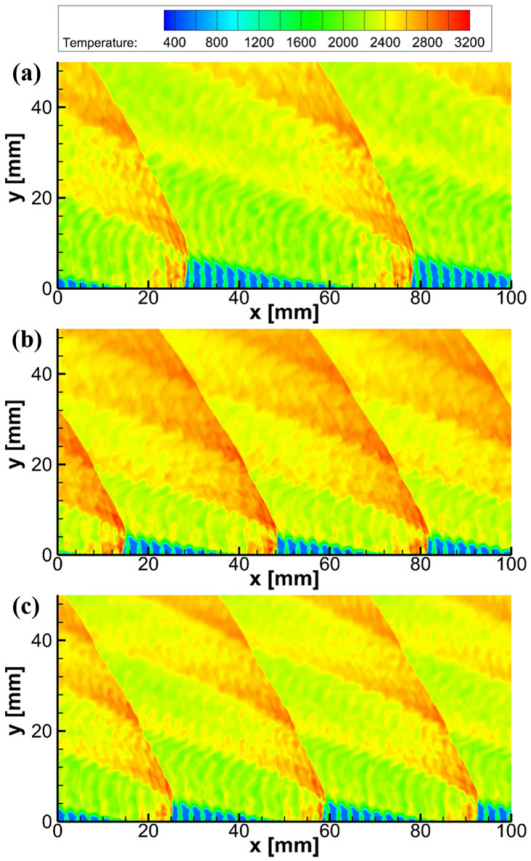

Figure 6. Temperature fields at = 600 K with different ozone additions: (**a**) φ = 0.1%; (**b**) φ = 1.0%; (**c**) φ = 2.0%.

Figure 7 illustrates the relationship between the RDW mode and the total temperature and ozone content φ. The x-axis and y-axis represent the ozone content, φ, and the number of detonation waves, respectively. At a total temperature of 300 K, a stable single wave and dual wave were obtained at φ = 0.1% and φ = 2.0%, respectively. However, at a total temperature of 400 K, the dual-wave mode was achieved at φ = 0.5%. At a total temperature of 500 K, as the flow field always maintained the dual-wave mode, the mode variation is not show in the Figure 7. In contrast, at a total temperature of 600 K, it appeared that the dual wave converted into triple wave when φ = 1.0%. These results suggest that a higher total temperature promotes the formation of multiple waves. The addition of ozone acts as an auxiliary initiation tool and can successfully initiate the reaction, which expands the operation range. The mode conversion from a single wave to multiple waves makes the flow structures and contact surface more stable. Therefore, the addition of ozone can also improve the stability of the flow field by changing the mode of the detonation wave. In the case where the inlet total temperature was 300 K, the addition of ozone led to a marked transition in the propagation mode of the detonation wave; this illustrates that the impact of ozone was even more evident under inflow conditions with a lower total temperature. Similarly, for a higher inlet total temperatures, a larger amount of ozone content is required to change the detonation wave mode.

The Cantera program, integrated with MATLAB and Python, was used to simulate the homogeneous isobaric ignition process in this work. The one-dimensional detonation ZND structure was calculated using SDtoolbox program, developed by Shepherd Group of California Institute of Technology. The induction time calculated theoretically is displayed in Figure 8.

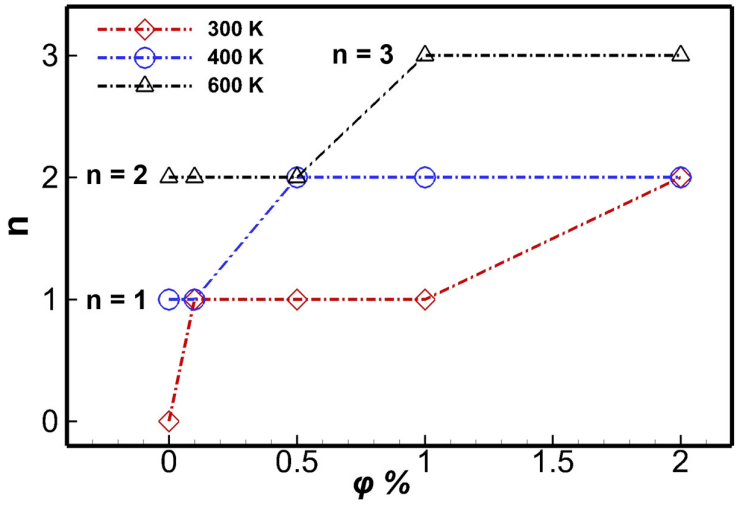

Figure 7. The number of detonation waves in different cases.

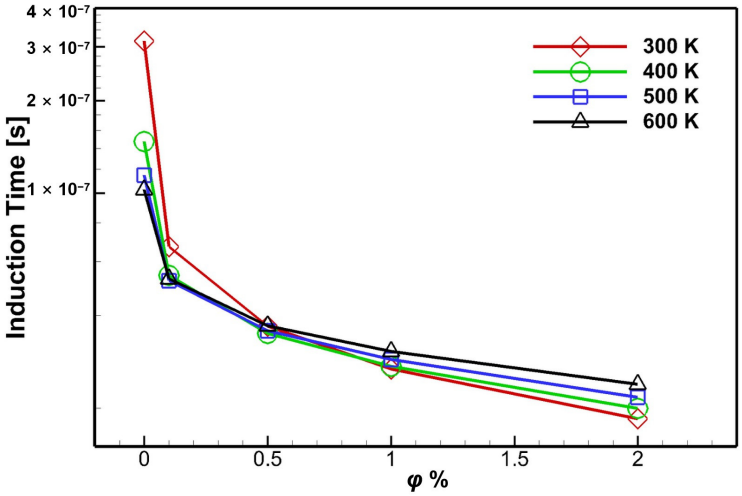

Figure 8. Theoretical induction time in different cases.

Based on the information provided, it appears that the induction time and number of waves in a reactive flow were affected by several factors, including inlet total temperature and ozone concentration. At φ = 0%, as the total temperature increased, the induction time decreased significantly, and the number of waves increased. For $\varphi \geq 0.1\%$, the theoretical induction time of the inflow at different total temperatures was roughly the same and lower than that of the inflow at 600 K without ozone addition. Kumar et al. [38] found that ignition promoters, such as O_3 and H_2O_2, can significantly shorten the induction length and time scale, which has a significant impact on the structure of the detonation, consistent with the results we calculated. This suggests that the effect of the induction time of the reactive gas ahead of the detonation wave on the detonation wave mode is not the primary factor. The formation of more hotspots for detonation wave is related to changes in the state of the inflow gas, including static temperature and velocity, as well as the interaction with the wall. The largest number of detonation waves occurred at T_{st} = 600 K. Additionally, the temperature of the banded products near the wall area increased as the total temperature increased, making it easier to create new hot spots and leading to an increase in detonation waves. It also seems that ozone acts as an ignition promoter, accelerating the reaction process and producing O radicals that speed up the chain branching, leading to the production of OH, a crucial indicator of the detonation reaction. This is consistent with the findings in Wang's study [39] in that ozone molecules decompose into O radicals, which accelerates the H-abstraction reactions during the combustion

process. Wang [39] found that the addition of ozone promotes the combustion process in hydrocarbon fuels by affecting the active free radicals and heat release rate. As a result, the increase in the ozone concentration has a more significant impact on the reaction rate and can lead to various forms of reactive flow fields. These observations suggest that the primary reason for both re-ignition and mode transition is the reduction in the induction time ahead of the wave. Ozone exhibits a more prominent impact on reducing the induction time of inflow with lower total temperature.

3.3. Discussion of Propagation Behaviors and Propulsion Performances

The propagation mode of the detonation combustion and propulsion performance are both crucial factors that need to be taken into account in the design of a combustion chamber. To explore the impact of ozone on detonation wave propagation, we conducted a statistical analysis for each case, as shown in Table 1. It should be noted that the value of the maximum heat release rate was obtained by statistically analyzing the entire computational domain. Since the heat release rate of the detonation combustion is much higher than that in regions such as the contact surface, the maximum heat release rate is often found in the reaction zone of the detonation wave. The results indicate that, as the total temperature increases, both the detonation propagation speed and maximum heat release rate decrease. However, our analysis suggests that ozone has a negligible effect on the detonation propagation speed and maximum heat release rate. Overall, an increase in the total temperature affects the heat release rate of detonation waves, resulting in a change in the propagation behavior, while ozone has been observed to have no significant effect on the propagation performance of detonation waves. By comparing Table 1 with Figure 7, we found that in the overall results, the detonation wave speed decreased as the wave number increased, and the effect of the wave number on the performance was not significant. This is consistent with the conclusion drawn by Daniel E. Paxson [40].

Table 1. Results of the speed of detonation wave and heat release rate.

		0%	**0.1%**	**0.5%**	**1.0%**
$V_d/\left(\mathrm{m}\cdot\mathrm{s}^{-1}\right)$	400 K	1875.1	1869.1	1811.2	1822.6
	600 K	1776.4	1707.3	1773.0	1763.4
$HRR/\left(\mathrm{J}\cdot\mathrm{s}^{-1}\right)$	400 K	5.21938×10^6	5.26051×10^6	5.07845×10^6	5.28373×10^6
	600 K	4.43678×10^6	4.27587×10^6	4.48233×10^6	4.36204×10^6

In order to evaluate the overall propulsion performance of the rotating detonation combustion with ozone addition, we calculated the total pressure and specific impulse at the outlet using Equation (7):

$$\dot{m}_R = \int_{Ai} \rho u dA_i$$

$$I_{sp} = \int_{Ao} \left[\rho u^2 + (p - p_b)\right] dA_o / (g\dot{m}_R) \tag{9}$$

where A_i and A_o are the area of the inlet and outlet; $\dot{m}_R$ is the mass flow rate of the fuel; g is the gravity acceleration; ρ, u, p, and p_b are density, velocity, pressure at the outlet and backpressure (taken as 1 atm in this work). Table 2 presents the total pressure P_{st} and specific impulse I_{sp} variations for the different cases. We found that the increase in the inlet total temperature led to a decrease in the total pressure at the outlet and an increase in the specific impulse. As the ozone concentration increased, it was observed that ozone had no significant effect on the total pressure at the outlet or the specific impulse in the combustion chamber. In general, while increasing both the total temperature and ozone concentration can increase the number of detonation waves, ozone has a negligible impact on the propulsion performance.

Table 2. Total pressure and specific impulse of the combustion outlet.

		0%	0.1%	0.5%	1.0%
P_{st}/MPa	400 K	0.538	0.533	0.528	0.527
	600 K	0.476	0.466	0.470	0.486
I_{sp}/s	400 K	209.5	206.4	201.3	201.7
	600 K	220.3	212.7	219.3	226.3

Under the inflow conditions of stoichiometric equivalence ratio, ozone had a negligible impact on the propagation behavior. Therefore, the study primarily focused on investigating the relationship between the ozone concentration and the propagation behavior of detonation waves under varying equivalence ratios at T_{st} = 300 K and P_{st} = 0.5 MPa. Additional cases were simulated to plot the boundary of the steady RDWs, as shown in Figure 9. For the case without ozone addition, the results indicate that steady RDWs can be obtained with an equivalence ratio close to 1.2. As shown in Figure 3, when the equivalence ratio is below 1.0, the presence of a recirculation zone leads to an unstable detonation wave. In contrast, a higher equivalence ratio results in a stronger detonation wave, which makes it difficult for fresh premixed gas to enter the chamber, causing the wave to extinguish. The addition of ozone results in more stable detonation waves, particularly at higher equivalence ratios, where ozone plays a critical role in stabilizing the detonation process. However, under lower equivalence ratios, ozone only acts as a supplementary factor in initiating detonation by reducing the induction time and accelerating the reaction. It should be noted that as the equivalence ratio decreases, a significantly higher ozone concentration is necessary to induce detonation, particularly when the ratio falls below the stoichiometric equivalence ratio.

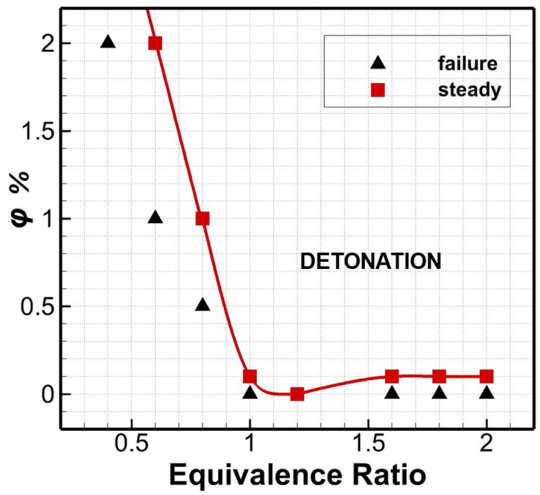

Figure 9. Equivalence ratio from 0.4 to 2.0 initiation results with O_3 addition.

4. Conclusions

In this paper, we presented two-dimensional numerical simulations of a Rotating Detonation Wave (RDW) with evenly distributed injection nozzles. With aim of exploring the influence of the total temperature and ozone on the rotating detonation modes, we simulated rotating detonation waves in hydrogen–air mixtures. The key conclusions of our study are as follows:

(1) Increasing the total temperature results in a corresponding increase in the number of detonation waves, which affects the behavior and performance of the RDE.

(2) The addition of ozone improves initiation results and can lead to a transition from single-wave to multi-wave detonation. Furthermore, ozone and an increase in the total

temperature result in smoother contact surfaces for the detonation waves, which can impact the stability of the combustion system.

(3) Ozone rapidly decomposes into O_2 and O, reducing the induction time of unburnt gas in front of the detonation by accelerating the reaction process.

(4) With an increase in the total temperature, there is a decrease in the speed of the detonation waves, maximum heat release rate, and total pressure at the exit, except for an increase in the specific impulse. However, ozone has no noticeable impact on detonation wave propagation behavior or propulsion performance.

(5) Ozone plays a significant role in determining the stability boundary of an RDE, especially at higher equivalence ratios, which means a small amount of ozone addition can improve the ignition result when the equivalence ratio is greater than one. At low equivalence ratios, there is an exponential increase in the demand for ozone to aid initiation, which broadens the operational range of the RDE.

Author Contributions: Conceptualization, Y.W. and C.T.; Methodology, C.T. and P.Y.; Software, Y.W. and C.T.; Validation, Y.W., C.T. and P.Y.; Formal analysis, Y.W., C.T. and P.Y.; Investigation, Y.W., C.T. and P.Y.; Resources, Y.W., C.T. and P.Y.; Data curation, Y.W.; Writing—original draft preparation, Y.W., C.T. and P.Y.; Writing—review and editing, Y.W., C.T. and P.Y.; Funding acquisition, C.T. and P.Y. All authors have read and agreed to the published version of the manuscript.

Funding: This research was funded by the National Natural Science Foundation of China, grant numbers: 12202014 and 12002041.

Data Availability Statement: All data used during the study appear in the submitted article.

Acknowledgments: We thank Honghui Teng for the invaluable assistance provided with computational resources.

Conflicts of Interest: The authors declare no conflict of interest.

References

1. Wolański, P. Detonative propulsion. *Proc. Combust. Inst.* **2013**, *34*, 125–158. [CrossRef]
2. Nlcholls, J.A.; Cullen, R.E.; Ragland, K.W. Feasibility studies of a rotating detonation wave rocket motor. *J. Spacecr. Rocket.* **1966**, *3*, 893–898. [CrossRef]
3. Yokoo, R.; Goto, K.; Kim, J.; Kawasaki, A.; Matsuoka, K.; Kasahara, J.; Matsuo, A.; Funaki, I. Propulsion performance of cylindrical rotating detonation engine. *AIAA J.* **2020**, *58*, 5107–5116. [CrossRef]
4. Xia, Z.; Ma, H.; Ge, G.; Zhou, C. Visual experimental investigation on initiation process of H_2/air rotating detonation wave in plane-radial structure. *Int. J. Hydrog. Energy* **2020**, *45*, 29579–29593. [CrossRef]
5. Meng, Q.; Zhao, N.; Zhang, H. On the distributions of fuel droplets and in situ vapor in rotating detonation combustion with prevaporized n-heptane sprays. *Phys. Fluids* **2021**, *33*, 043307. [CrossRef]
6. Rankin, B.A.; Fotia, M.L.; Naples, A.G.; Stevens, C.A.; Hoke, J.L.; Kaemming, T.A.; Theuerkauf, S.W.; Schauer, F.R. Overview of performance, application, and analysis of rotating detonation engine technologies. *J. Propuls. Power* **2017**, *33*, 131–143. [CrossRef]
7. Lu, F.K.; Braun, E.M. Rotating detonation wave propulsion: Experimental challenges, modeling, and engine concepts. *J. Propuls. Power* **2014**, *30*, 1125–1142. [CrossRef]
8. Viotsehkovsky, B.V. Stationary spin detonation. *Sov. J. Appl. Mech. Tech. Phys.* **1960**, *3*, 157–164.
9. Bykovskii, F.A.; Zhdan, S.A.; Vedernikov, E.F. Continuous spin detonations. *J. Propuls. Power* **2006**, *22*, 1204–1216. [CrossRef]
10. Bykovskii, F.A.; Vedernikov, E.F. Continuous detonation combustion of an annular gas-mixture layer. *Combust. Explos. Shock. Waves* **1996**, *32*, 489–491. [CrossRef]
11. Bykovskii, F.A.; Mitrofanov, V.V. A continuous spin detonation in liquid fuel sprays. In *Control of Detonation Processes*; Elex-KM Publ.: Moscow, Russia, 2000; pp. 209–211.
12. Zhou, R.; Wang, J.P. Numerical investigation of shock wave reflections near the head ends of rotating detonation engines. *Shock Waves* **2013**, *23*, 461–472. [CrossRef]
13. Yi, T.H.; Lou, J.; Turangan, C.; Choi, J.Y.; Wolanski, P. Propulsive performance of a continuously rotating detonation engine. *J. Propuls. Power* **2011**, *27*, 171–181. [CrossRef]
14. Uemura, Y.; Hayashi, A.K.; Asahara, M.; Tsuboi, N.; Yamada, E. Transverse wave generation mechanism in rotating detonation. *Proc. Combust. Inst.* **2013**, *34*, 1981–1989. [CrossRef]
15. Ma, Z.; Zhang, S.; Luan, M.; Yao, S.; Xia, Z.; Wang, J. Experimental research on ignition, quenching, reinitiation and the stabilization process in rotating detonation engine. *Int. J. Hydrog. Energy* **2018**, *43*, 18521–18529. [CrossRef]
16. Zhao, M.; Li, J.M.; Teo, C.J.; Khoo, B.C.; Zhang, H. Effects of Variable Total Pressures on Instability and Extinction of Rotating Detonation Combustion. *Flow Turbul. Combust.* **2020**, *104*, 261–290. [CrossRef]

17. Jourdaine, N.; Tsuboi, N.; Ozawa, K.; Kojima, T.; Hayashi, A.K. Three-dimensional numerical thrust performance analysis of hydrogen fuel mixture rotating detonation engine with aerospike nozzle. *Proc. Combust. Inst.* **2019**, *37*, 3443–3451. [CrossRef]
18. Liu, X.Y.; Cheng, M.; Zhang, Y.Z.; Wang, J.P. Design and optimization of aerospike nozzle for rotating detonation engine. *Aerosp. Sci. Technol.* **2022**, *120*, 107300. [CrossRef]
19. Eto, S.; Tsuboi, N.; Kojima, T.; Hayashi, A.K. Three-dimensional numerical simulation of a rotating detonation engine: Effects of the throat of a converging-diverging nozzle on engine performance. *Combust. Sci. Technol.* **2016**, *188*, 2105–2116. [CrossRef]
20. Shao, Y.; Liu, M.; Wang, J. Continuous detonation engine and effects of different types of nozzle on its propulsion performance. *Chin. J. Aeronaut.* **2010**, *23*, 647–652. [CrossRef]
21. Huang, Y.; Xia, H.; Chen, X.; Luan, Z.; You, Y. Shock dynamics and expansion characteristics of an aerospike nozzle and its interaction with the rotating detonation combustor. *Aerosp. Sci. Technol.* **2021**, *117*, 106969. [CrossRef]
22. Zhu, Y.; Wang, K.; Wang, Z.; Zhao, M.; Jiao, Z.; Wang, Y.; Fan, W. Study on the performance of a rotating detonation chamber with different aerospike nozzles. *Aerosp. Sci. Technol.* **2020**, *107*, 106338. [CrossRef]
23. Huang, Z.; Zhao, M.; Zhang, H. Modelling n-heptane dilute spray flames in a model supersonic combustor fueled by hydrogen. *Fuel* **2020**, *264*, 116809. [CrossRef]
24. Kindracki, J. Study of detonation initiation in kerosene–oxidizer mixtures in short tubes. *Shock Waves* **2014**, *24*, 603–618. [CrossRef]
25. Kindracki, J. Experimental research on rotating detonation in liquid fuel–gaseous air mixtures. *Aerosp. Sci. Technol.* **2015**, *43*, 445–453. [CrossRef]
26. Zhao, M.; Ren, Z.; Zhang, H. Pulsating detonative combustion in n-heptane/air mixtures under off-stoichiometric conditions. *Combust. Flame* **2021**, *226*, 285–301. [CrossRef]
27. Fotia, M.L.; Schauer, F.; Kaemming, T.; Hoke, J. Experimental study of the performance of a rotating detonation engine with nozzle. *J. Propuls. Power* **2016**, *32*, 674–681. [CrossRef]
28. Zhao, H.; Yang, X.; Ju, Y. Kinetic studies of ozone assisted low temperature oxidation of dimethyl ether in a flow reactor using molecular-beam mass spectrometry. *Combust. Flame* **2016**, *173*, 187–194. [CrossRef]
29. Han, W.; Liang, W.; Wang, C.; Wen, J.X.; Law, C.K. Spontaneous initiation and development of hydrogen-oxygen detonation with ozone sensitization. *Proc. Combust. Inst.* **2021**, *38*, 3575–3583. [CrossRef]
30. Sun, W.; Gao, X.; Wu, B.; Ombrello, T. The effect of ozone addition on combustion: Kinetics and dynamics. *Prog. Energy Combust. Sci.* **2019**, *73*, 1–25. [CrossRef]
31. Burke, M.P.; Chaos, M.; Ju, Y.; Dryer, F.L.; Klippenstein, S.J. Comprehensive H_2/O_2 kinetic model for high-pressure combustion. *Int. J. Chem. Kinet.* **2012**, *44*, 444–474. [CrossRef]
32. Kurganov, A.; Noelle, S.; Petrova, G. Semidiscrete central-upwind schemes for hyperbolic conservation laws and Hamilton—Jacobi equations. *SIAM J. Sci. Comput.* **2001**, *23*, 707–740. [CrossRef]
33. Liu, Y.; Wang, Y.; Li, Y.; Li, Y.; Wang, J. Spectral analysis and self-adjusting mechanism for oscillation phenomenon in hydrogen-oxygen continuously rotating detonation engine. *Chin. J. Aeronaut.* **2015**, *28*, 669–675. [CrossRef]
34. Yao, K.; Yang, P.; Teng, H.; Chen, Z.; Wang, C. Effects of injection parameters on propagation patterns of hydrogen-fueled rotating detonation waves. *Int. J. Hydrog. Energy* **2022**, *47*, 38811–38822. [CrossRef]
35. Chacon, F.; Gamba, M. OH PLIF visualization of an optically accessible rotating detonation combustor. In Proceedings of the AIAA Propulsion and Energy 2019 Forum, Indianapolis, IN, USA, 19–22 August 2019; p. 4217. [CrossRef]
36. Chacon, F.; Gamba, M. Study of parasitic combustion in an optically accessible continuous wave rotating detonation engine. In Proceedings of the AIAA Scitech 2019 Forum, San Diego, CA, USA, 7–11 January 2019; p. 0473. [CrossRef]
37. Cocks, P.A.; Holley, A.T.; Rankin, B.A. High fidelity simulations of a non-premixed rotating detonation engine. In Proceedings of the 54th AIAA Aerospace Sciences Meeting, San Diego, CA, USA, 4–8 January 2016; p. 0125. [CrossRef]
38. Kumar, D.S.; Ivin, K.; Singh, A.V. Sensitizing gaseous detonations for hydrogen/ethylene-air mixtures using ozone and H_2O_2 as dopants for application in rotating detonation engines. *Proc. Combust. Inst.* **2021**, *38*, 3825–3834. [CrossRef]
39. Wang, Z.; Yan, C.; Lin, Y.; Zhou, M.; Jiang, B.; Liu, N.; Zhong, H.; Ju, Y. Kinetics and extinction of non-premixed cool and warm flames of dimethyl ether at elevated pressure. *Proc. Combust. Inst.* **2022**, *in press*. [CrossRef]
40. Paxson, D.E. Computational Assessment of the Impact of Wave Count on Rotating Detonation Engine Performance. In Proceedings of the AIAA SCITECH 2023 Forum, National Harbor, MD, USA, 23–27 January 2023; p. 1290. [CrossRef]